Communication

Bifocal Fresnel Lens Based on the Polarization-Sensitive Metasurface

Hen Markovich, Dmitrii Filonov, Ivan Shishkin, and Pavel Ginzburg

***Abstract*— Thin structured surfaces allow flexible control over the propagation of electromagnetic waves. Focusing and polarization state analysis are among functions, required for effective manipulation of radiation. Here, a polarization-sensitive Fresnel zone plate lens is proposed and experimentally demonstrated for gigahertz spectral range. Two spatially separated focal spots for orthogonal polarizations are obtained by designing metasurface pattern, made of overlapping tightly packed cross- and rod-shaped antennas with a strong polarization selectivity. The optimized subwavelength pattern allows multiplexing two different lenses with low polarization crosstalk on the same substrate and provides a control over focal spots of the lens only by changing the polarization state of the incident wave. More than a wavelength separation distance between the focal spots was demonstrated for a broad spectral range, covering half a decade in frequency. The proposed concept could be straightforwardly extended for terahertz and visible spectra, where polarization-sensitive elements utilize localized plasmon resonance phenomenon.**

***Index Terms*— Artificial media, focusing, lenses, metasurfaces.**

I. Introduction

Control over the propagation of electromagnetic waves with thin subwavelength patterned surfaces is required in a broad range of applications. This approach enables a significant reduction of both volumes and weights of devices used in wireless communication links. Impedance surfaces and related approaches are usually utilized for those purposes [1]. Different types of reflect-, transmit-, and phase-shifting arrays and surfaces are commonly employed for tailoring properties of electromagnetic radiation at gigahertz frequency range (see [2], [3]). The proposed device falls into the transmit array category with an additional binary function, as it will be shown hereafter.

A recent interest in structured surfaces with carefully designed patterns was partially inspired by a series of works on optical metasurfaces (see [4]–[6], [7]), which allow flexible control over light propagation with nanometer-thin layers (also [8] for general concepts of tailoring reflection and transmission coefficients with resonant structures). Subwavelength elements, forming a metasurface pattern, utilize localized plasmon resonance phenomenon, which allows achieving desired properties by means of geometrical tuning of nanoantennas' shapes (see [9], [10]). Essential requirement to be met for achieving a broad range of functions is the ability to obtain a full phase control upon an interaction with individual elements (or small arrays of those) (see [5]).

The recent progress in optical imaging with metasurfaces along with the development of new concepts in field manipulation with thin elements inspired the development of new systems, operating at microwave regimes. Radio frequency (RF) imaging techniques, widely employed in the traditional radar applications [11], are utilized nowadays for advancing volumetric scanning in a cluttered environment [12]. For example, 3-D images of a crowd in public places are acquired at 30–300 GHz frequency band for security reasons (see [13]). Flat elements, capable of fast data analysis, are required for performing the processing. Furthermore, specular and diffusive reflections from irregular surfaces may result in a loss of information. Consequently, a significant coverage of stereo angles with detecting systems is required. While bulky and mechanically movable antennas cannot be used for these purposes from practical standpoints, cheap, flat, and integrable elements should be employed. Lenses are essential elements, required for standard imaging techniques. As a remark, computational imaging could relax this demand (see [14]).

Microwave lensing is intensively studied over the last 50 years [15]. Flat lenses are usually made of either single [16] or multilayered sheets of metal patterns, with electric connections between them [17], [18] or without [19], [20]. Negative index metamaterials can also be employed [21]. Recently, metasurface-based lenses implemented on flexible substrates have been demonstrated [22]. A significant benefit of metasurface-based approach (for all frequency ranges) is the minimization of the thickness of the structures. It found its use in variety of applications, like beam formation at several angles for different polarizations [23], a single focal spot for different wavelengths [24], correction of chromatic aberrations [25], beam steering [26], and beam shaping [27] to name just a few (see [28] for general design principles). Axial stacking of multiple layers one on the top of the other is beneficial for achieving the goals of those designs [29]. Many applications require flexible control over a broader span of phases with a wavefront, covering the range $[-\pi, \pi]$, including abilities to design spatial discontinuities in parameters. This functionality, however, strongly depends on the illumination frequency. The broadband operation can be achieved by cascading several resonant systems, as it is usually done in the field.

Here, the general approach of functional superposition in order to focus two orthogonal polarizations into a pair of different spatially separated focal points will be undertaken. While the polarization degree of freedom was routinely exploited in many configurations, based on refraction engineering, bifocal lensing was not demonstrated. This function is required for a special class of devices, which perform imaging and/or analysis of cross-polarized states simultaneously. For example, the direction of arrival detection and polarization state analysis is among the possible applications. The first function, for example, is highly demanded in designs of adoptive antennas [1]. Phased arrays are usually used for this purpose, but require a set of expensive electronic elements [1]. The proposed design capable of analyzing the state with a pair of phased locked detectors, situated at two focal planes. Furthermore, the focal length of the designed lens is only a few wavelengths, which makes the entire device to be relatively compact. For the summary, the functionality of focal positions discrimination for mutually orthogonal polarizations is depicted in Fig. 1. The polarization-sensitive 2-D

Manuscript received July 17, 2017; revised December 7, 2017; accepted February 28, 2018. Date of publication March 6, 2018; date of current version May 3, 2018. This work was supported in part by TAU Rector Grant, in part by PAZY Foundation, and in part by Kamin Project. *(Hen Markovich, Dmitrii Filonov, and Ivan Shishkin contributed equally to this work.) (Corresponding author: Hen Markovich.)*

The authors are with the School of Electrical Engineering, Tel Aviv University, Tel Aviv 69978, Israel (e-mail: henmarkovich@mail.tau.ac.il; dmitriy.filonov@phoi.ifmo.ru; ivanshishkin@post.tau.ac.il; pginzburg@post.tau.ac.il).

Color versions of one or more of the figures in this communication are available online at http://ieeexplore.ieee.org.

Digital Object Identifier 10.1109/TAP.2018.2811717

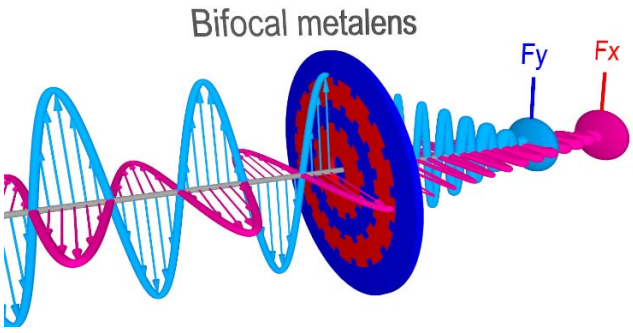

Fig. 1. Bifocal Fresnel zone plate lens—two orthogonal polarizations are focused at different points along the propagation axis owing to interactions with polarization-sensitive overlapping metasurface-based Fresnel zones.

pattern is implemented on a single printed circuit board (PCB) and optimized towards spatial separation of focal spots.

This communication is organized as follows. The design concept is followed by numerical and experimental results. The comparison with standard Fresnel lens formulas comes before the concluding remarks and the outlook.

II. Bifocal Lens Design

The bifocal lens design utilizes the basic Fresnel zone plate concept. A set of alternating opaque-transparent concentric rings are either blocking or transmitting the incident electromagnetic wave. The focus of the lens is formed owing to the interference of the transparent Fresnel zones. On the contrary to conventional dielectric lenses based on quadratic phase accumulation, the zone plate device provides a flat and cheap solution with a drawback of 50% back reflection of energy, which is virtually lost in imaging applications. Fresnel zones defined with the following set of radii [30]:

$$r_n = \sqrt{n\lambda F + \frac{n^2\lambda^2}{4}} \tag{1}$$

where n is the number of the zone, λ is the wavelength that the lens is designed for, F is the focal distance of the lens, and r_n is the outer radius of the nth ring, also corresponding to the inner radius of the $n+1$th ring. Relation (1) explicitly shows that the Fresnel radii depend on the focal distance and, hence, in order to achieve multiple focal points several types of zones should be overlapping. It can be realized by stacking multiple decoupled zone plate lenses one on the top of the other or by using the polarization degree of freedom of electromagnetic waves—this approach will be followed hereafter.

A basic scheme of the lens is shown in Fig. 1(a)—flat structure provides two distinguishably different focal points along the optical axis of the system. The polarization-sensitive response of a structured surface is achieved by designing elongated patches, which interact with one predefined polarization. Individual meta-atoms are subwavelength and are not resonant with the incident polarization—this is the key for a broadband operation of the device, which will be demonstrated hereafter. The orthogonal component of the field weakly interacts with the short axis of a patch and, as a result, polarization-dependent opaqueness or transparency is achieved. In the region, where Fresnel zones for both polarizations overlap (recall different focal distance influences), orthogonal patches will create cross-shaped planar antennas. Here, a careful optimization of the design is needed in order to prevent cross-polarization coupling. Details of the optimization routine will be described hereafter.

The lens was designed to operate at 10 GHz central frequency and to provide two focal spots for different polarizations located at $F_y = 90$ mm $= 3\lambda$ (Y lens) and $F_x = 150$ mm $= 5\lambda$ (X lens)

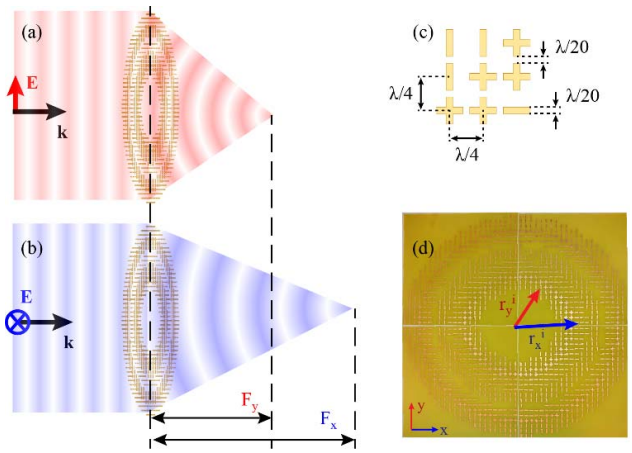

Fig. 2. Bifocal Fresnel lens—the concept and design. (a) and (b) Schematics of bifocal operation—orthogonal linear polarizations are focused at different distances from the flat patterned surface. (c) Single cell's characteristic dimensions: horizontal, vertical, and cross-shaped patches. (d) Photograph of the fabricated lens—four PCB plates form a 328 mm × 328 mm flat lens.

TABLE I
Zone Plates Zones Radii in Millimeter (in Wavelength)

$\mathbf{r_n}$	X Polarization	Y Polarization
r_1	68.74mm (2.29)	54.08mm (1.8)
r_2	99.5mm (3.32)	79.37mm (2.65)
r_3	124.6mm (4.15)	100.62mm (3.35)
r_4	146.97mm (4.9)	120mm (4)
r_5	--	138.29mm (4.61)
r_6	--	155.88mm (5.2)

from the patterned surface—the focal points are separated by two wavelengths. Fig. 2(a) and (b) schematically shows the positions of the focal spots depending on the polarization of the incident field. Such a separation should result in two distinguishable and measurable spots in the field distribution. Y lens consisted of six zones (filled even zones) and X lens was made of four zones (filled even zones) [Fig. 2(d)]. The relevant parameters are summarized in Table I.

General metasurface design rules should consider a number of effects beyond classical homogenization model [31] and further numerical optimization are beneficial for achieving desired performances [32]. Here, the latter approach was employed. Optimization and performance evaluation of the lens design was done numerically with CST Microwave studio ("time domain solver," ~ 2.4 mesh cells per mm^3). The optimization of the metasurface properties was made in order to reduce polarization crosstalk and minimize sizes of focal spots [depth of focus (DOF) in the z-direction]. It was performed numerically using parameter sweep on the whole lens with a finite number of elements. The maximal field intensity at the focal spot was optimized by sweeping the width and length of patch antennas and their period. The number of Fresnel zones was constrained by available sizes of the "on shelf" PCB plates (four 170 mm × 170 mm plates were stitched together in the final realization). Finally, the metal patches dimensions were selected to be $\lambda/5$ by $\lambda/20$, which yielded the values of 6 and 1.5 mm correspondingly for 10 GHz frequency [Fig. 2(c)]. The gap between the two adjacent rods was chosen to be 1.5 mm ($\lambda/20$). The total size of each metasurface cell is 7.5 mm ($\lambda/4$) by 7.5 mm ($\lambda/4$). Fig. 2(c) shows the design of vertical, horizontal, and overlapping regions. Electromagnetic properties of substrates,

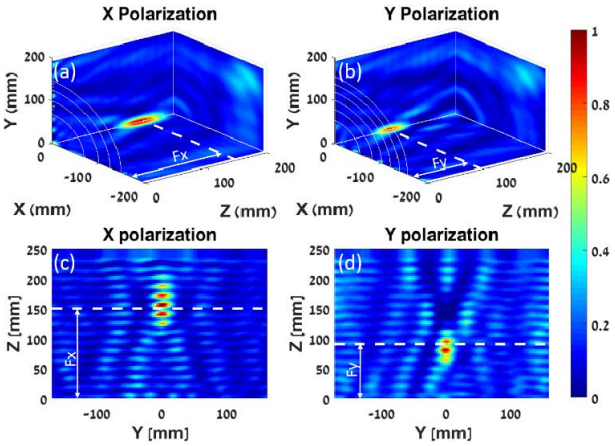

Fig. 3. Transmitted electric field intensity (the scale is normalized to the maximum intensity) distributions after the bifocal Fresnel lens, illuminated with a 10 GHz plane wave. White dashed lines indicate positions of the highest intensity (focal position along the optical axis). Numerical data for (a) X-polarized incident wave and (b) Y-polarized incident wave. Electric field intensity distribution after the lens in the *yz* plane—experimental data (c) X-polarized incident wave and (d) Y-polarized incident wave.

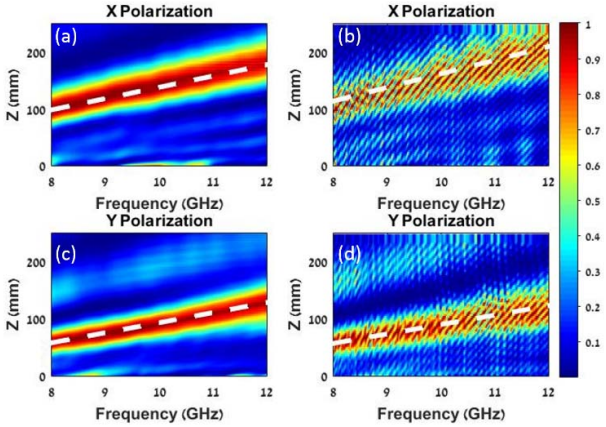

Fig. 4. Electric field intensity (the scale is normalized to the maximum intensity of each frequency) distribution along the optical axis of the lens (vertical lines) for frequencies range between 8 and 12 GHz (horizontal axis). The color map is normalized to the same value. The white dashed lines follow the maximum of the field intensity (the focal spot). Numerical data for (a) X polarization and (c) Y polarization. Experimental data for (b) X polarization and (d) Y polarization.

used in the experimental demonstration (copper-plated PCB, copper (conductivity of 5.96×10^7 S/m) of thickness—100 μm ($\lambda/300$) and substrate—1.5 mm ($\lambda/20$) of FR-4 glass epoxy (permittivity of 4.3, tg(δ) of 0.018), were introduced for obtaining the optimized design.

It is worth noting that in terms of antenna terminology, the focal point lies in the reactive region of the structure. Majority of the reported Fresnel lenses, designed for the millimeter waves, do operate in this area, which, in principle, might affect the imaging capabilities of the device (see [33]). Nevertheless, if the energy harvesting function is required, short focal length is beneficial for achieving compact designs. The overall bandwidth of the device was not optimized and will be shown to be around 0.5 GHz, which is sufficient for low gigahertz applications and comparable with other reports in the field (see [34]).

III. Results

The lens was fabricated with a help of photolithography, followed by etching of copper-plated PCBs. A wideband horn antenna (IDPH2018, 2–18 GHz), connected to the transmitting port of a vector network analyzer (VNA, Agilent E8362B), was used as a plane wave excitation source. The lens is located at the far-field zone of the antenna (2.5 m apart). The fields were measured with a 3-D near-field scanner. An electrical field probe was mounted on the scanner and connected to the receiving port of the VNA. The shielded aperture of the probe has a 2 mm diameter and could be approximated as an electrically small perturbation that measures electrical fields along a given direction, without performing a significant field averaging. In the case of study here, the probe was oriented normally to the incident k-vector and parallel to the dominant electric component of the field radiated from the horn. The near-field mapping is performed over a rectangular area (250 mm $\times$ 350 mm) with 3 mm steps ($\lambda/10$) in both (y and z) directions starting at 2 mm offset from the back interface of the lens, in order to avoid a contact between the probe and the sample.

Fig. 3(a) and (b) shows numerically obtained electric field intensity distributions for two different polarizations of the incident plane wave. Two well distinguishable focal spots can be observed and follow the initial design requirements. It can be seen that X-polarized wave shows the larger DOF—the focal spot is extended along the optical axis. This effect is attributed to different focal lengths and the different number of Fresnel zones, used for X- and Y-polarizations (150 mm with four zones and 90 mm with six zones, correspondingly), as will be discussed later. Fresnel zone plates also create a back reflected focal spot, which is situated at the same distance as the forward focus, but in the negative direction along the optical axis. Numerical modeling (not shown here) clearly indicates its existence. The proposed design demonstrates about 34% and 40% overall reflection for X- and Y-polarizations accordingly, as it was evaluated numerically at 10 GHz, while 3.4% and 2.56% power harvesting to the focal spot is estimated. Furthermore, additional diffraction orders form secondary focuses, as it is expected from a binary Fresnel zone designs [35].

The numerical data can be directly compared with the experimentally obtained near-field scans in the *yz* plane [Fig. 3(c) and (d)]. While the same focal positions were obtained in both numerical and experimental cases, the latter one demonstrates nonuniform (wavy) distribution of the field in the focal spot. The clearly distinguishable periodicity corresponds to the wavelength of the excitation and is quite typical for experiments, performed in an anechoic chamber. The ripples along the Z-axis are created by interference of the transmitted field with the reflections from the metallic parts of the 3-D scanner.

Equation (1) clearly demonstrates a strong chromatic dependence of the focal positions. Nevertheless, spatial separation of focuses for orthogonal polarizations still holds for different frequencies of the incident wave. This bifocal performance in the range of 8–12 GHz will be tested next. The results of the frequency sweep measurements are presented in Fig. 4, which demonstrates the intensity scans along the optical axis for the chosen frequency range. Each vertical line stands for one scan per frequency and it was normalized to its peak field value. As it can be observed in both numerical and the experimental investigations, the focal positions F_x and F_y do move as the function of frequency, nevertheless spatial separation between them is preserved. Experimental data suffer from the same wavy behavior, observed in the 3-D field scans [Fig. 3(c) and (d)]. The slopes of the white dashed lines (main focal positions) in both of the cases are nearly identical, which results in a constant distance between X- and Y-focal spots (~60 mm). As expected, higher and lower order focuses, located farther and closer to the main focal spot

TABLE II
SUMMARY OF THE BIFOCAL LENS PARAMETERS—THEORETICAL VALUES APPEAR AT THE UPPER ROWS OF EACH CELL, WHILE EXPERIMENTAL DATA ARE ENCLOSED IN ROUND BRACKETS AND THE NUMERICAL DATA IN SQUARE BRACKETS

	X Polarization – (N=4)		Y Polarization – (N=6)	
ω_{in}	$F(\omega_{incident})$	DOF	$F(\omega_{incident})$	DOF
8 GHz	112.5mm (~105mm) [~100mm]	±14.06mm (~±25mm) [~±23mm]	67.5mm (~55mm) [~55mm]	±5.63mm (~±15mm) [~±15mm]
10 GHz	150mm (~155mm) [~±145mm]	±18.75mm (~±30mm) [~±27mm]	90mm (~90mm) [~90mm]	±7.5mm (~±23mm) [~±20mm]
12 GHz	175mm (~200mm) [~185mm]	±21.88mm (~±35mm) [~±25mm]	105mm (~115mm) [~130mm]	±8.75mm (~±30mm) [~±25mm]

could be distinguished. It is a well-known phenomenon of binary Fresnel zone plates that a small part of the transmitted power of the lens goes into odd-orders focal spots [35].

The shift of the focal position with the frequency change is given by the following approximation [30]

$$F(\omega_{\text{incident}}) \cong F_{\text{designed}} \left(2 - \frac{\omega_{\text{designed}}}{\omega_{\text{incident}}}\right) \tag{2}$$

where F_{designed} and ω_{designed} are the focal distance and the frequency, respectively, that the lens is designed for. ω_{incident} is the actual frequency of the incident plane wave, and $F(\omega_{\text{incident}})$ is the calculated/measured focal distance of the lens for incident wave with frequency ω_{incident}.

The DOF could be approximated by [30]

$$\text{DOF} \cong \pm \frac{F(\omega_{\text{incident}})}{2N} \tag{3}$$

where DOF is the depth of focus (± stays for distances spread from the center of the focal point) and N is the number of zones related to the wave polarization. In the bifocal design, both F and N are different for orthogonal polarizations.

Both of (2) and (3) are valid approximations for the case, when $N\lambda F \gg ((N\lambda/2))^2$ [recall the expressions in (1)]. This condition is satisfied relatively well in the current design (factor of ~3 in the ratio). The parameters of the bifocal lens are summarized in Table II. Values, calculated with (2) and (3) along with those, extracted from actual measurements (those numbers appear in round brackets) and those extracted from the numerical simulation (appears in square brackets) can be directly compared. It can be seen that the results agree relatively well and the differences between the simulation and the measured results are in the range of ~10%.

IV. CONCLUSION

The approach toward creation of polarization-sensitive bifocal lens has been demonstrated both numerically and experimentally. The Fresnel zone plate lens has been used as a basis for the studies. It was demonstrated that the zone plate lens consisting of subwavelength metal patches yields polarization sensitivity of the focal spot position. The versatility of the approach was supported by the studies of the lens performances in the wide frequency range (8–12 GHz). The proposed lens design is susceptible to chromatic aberration, though it provides the stability in the relation between focal positions for different polarizations, which might be useful for polarization state mapping and RF imaging in orthogonal polarizations simultaneously. The design rules could be used for demonstration similar performances at the optical spectral range. Furthermore, RF designs could serve as emulation tools for studies of complex photonic phenomena, where both fabrication and characterization are resource-consuming (see [36]–[38]). In terms of RF applications, the proposed design can serve as a basis for polarization state analyzing and direction of arrival devices, where large apertures for improved signal-to-noise ratios are required. The concept of binary transmit array surfaces can be further extended towards multilevel functionalities, which can find a use in many applications in a broad spectral range.

REFERENCES

[1] C. A. Balanis, *Antenna Theory: Analysis and Design*, 3rd ed. Hoboken, NJ, USA: Wiley, 2005.

[2] D. M. Pozar, S. D. Targonski, and H. D. Syrigos, "Design of millimeter wave microstrip reflectarrays," *IEEE Trans. Antennas Propag.*, vol. 45, no. 2, pp. 287–296, Feb. 1997.

[3] N. Gagnon, A. Petosa, and D. A. McNamara, "Research and development on phase-shifting surfaces (PSSs)," *IEEE Antennas Propag. Mag.*, vol. 55, no. 2, pp. 29–48, Apr. 2013.

[4] N. Shitrit *et al.*, "Spin-optical metamaterial route to spin-controlled photonics," *Science*, vol. 340, no. 6133, pp. 724–726, May 2013.

[5] N. Yu and F. Capasso, "Flat optics with designer metasurfaces," *Nature Mater.*, vol. 13, pp. 139–150, Jan. 2014.

[6] A. V. Kildishev, A. Boltasseva, and V. M. Shalaev, "Planar photonics with metasurfaces," *Science*, vol. 339, no. 6125, p. 1232009, Mar. 2013.

[7] S. B. Glybovski, S. A. Tretyakov, P. A. Belov, Y. S. Kivshar, and C. R. Simovski, "Metasurfaces: From microwaves to visible," *Phys. Rep.*, vol. 634, pp. 1–72, May 2016.

[8] C. L. Holloway, M. A. Mohamed, E. F. Kuester, and A. Dienstfrey, "Reflection and transmission properties of a metafilm: With an application to a controllable surface composed of resonant particles," *IEEE Trans. Electromagn. Compat.*, vol. 47, no. 4, pp. 853–865, Nov. 2005.

[9] N. Berkovitch, P. Ginzburg, and M. Orenstein, "Nano-plasmonic antennas in the near infrared regime," *J. Phys., Condens. Matter*, vol. 24, no. 7, p. 73202, 2012.

[10] P. Ginzburg, N. Berkovitch, A. Nevet, I. Shor, and M. Orenstein, "Resonances on-demand for plasmonic nano-particles," *Nano Lett.*, vol. 11, no. 6, pp. 2329–2333, 2011.

[11] M. A. Richards, *Fundamentals of Radar Signal Processing*, 2nd ed. New York, NY, USA: McGraw-Hill, 2014.

[12] J. Hunt *et al.*, "Metamaterial microwave holographic imaging system," *J. Opt. Soc. Amer. A*, vol. 31, no. 10, pp. 2109–2119, Oct. 2014.

[13] M. Caris *et al.*, "Very high resolution radar at 300 GHz," in *Proc. 44th Eur. Microw. Conf.*, Oct. 2014, pp. 1797–1799.

[14] T. Fromenteze *et al.*, "Computational imaging using a mode-mixing cavity at microwave frequencies," *Appl. Phys. Lett.*, vol. 106, no. 19, p. 194104, 2015.

[15] W. Rotman and R. Turner, "Wide-angle microwave lens for line source applications," *IEEE Trans. Antennas Propag.*, vol. 11, no. 6, pp. 623–632, Nov. 1963.

[16] M. Casaletti, M. Śmierzchalski, M. Ettorre, R. Sauleau, and N. Capet, "Polarized beams using scalar metasurfaces," *IEEE Trans. Antennas Propag.*, vol. 64, no. 8, pp. 3391–3400, Aug. 2016.

[17] H. Kaouach and A. Kabashi, "Simple tri-layer linearly polarized discrete lens antenna with high-efficiency for mmWave applications," *IEEE Antennas Wireless Propag. Lett.*, vol. 15, pp. 259–262, 2016.

[18] C. Jouanlanne *et al.*, "Wideband linearly polarized transmitarray antenna for 60 GHz backhauling," *IEEE Trans. Antennas Propag.*, vol. 65, no. 3, pp. 1440–1445, Mar. 2017.

[19] C. Pfeiffer and A. Grbic, "Planar lens antennas of subwavelength thickness: Collimating leaky-waves with metasurfaces," *IEEE Trans. Antennas Propag.*, vol. 63, no. 7, pp. 3248–3253, Jul. 2015.

[20] Q. L. Li, S. W. Cheung, D. Wu, and T. I. Yuk, "Microwave lens using periodic dielectric sheets for antenna-gain enhancement," *IEEE Trans. Antennas Propag.*, vol. 65, no. 4, pp. 2068–2073, Apr. 2017.

[21] I. M. Ehrenberg, S. E. Sarma, and B.-I. Wu, "A three-dimensional self-supporting low loss microwave lens with a negative refractive index," *J. Appl. Phys.*, vol. 112, no. 7, pp. 1–5, 2012.

[22] Y. Zárate, I. V. Shadrivov, and D. A. Powell, "Tunable focusing by a flexible metasurface," *Photon. Nanostruct.-Fundam. Appl.*, vol. 26, pp. 62–68, Sep. 2017.
[23] K. Pham *et al.*, "Design of wideband dual linearly polarized transmitarray antennas," *IEEE Trans. Antennas Propag.*, vol. 64, no. 5, pp. 2022–2026, May 2016.
[24] O. Eisenbach, O. Avayu, R. Ditcovski, and T. Ellenbogen, "Metasurfaces based dual wavelength diffractive lenses," *Opt. Exp.*, vol. 23, no. 4, p. 3928, 2015.
[25] O. Avayu, E. Almeida, Y. Prior, and T. Ellenbogen, "Composite functional metasurfaces for multispectral achromatic optics," *Nature Commun.*, vol. 8, p. 14992, Apr. 2017.
[26] T. Cai *et al.*, "Ultra-thin polarization beam splitter using 2-D transmissive phase gradient metasurface," *IEEE Trans. Antennas Propag.*, vol. 63, no. 12, pp. 5629–5636, Dec. 2015.
[27] O. Avayu, O. Eisenbach, R. Ditcovski, and T. Ellenbogen, "Optical metasurfaces for polarization-controlled beam shaping," *Opt. Lett.*, vol. 39, no. 13, pp. 3892–3895, Jul. 2014.
[28] K. Achouri, B. A. Khan, S. Gupta, G. Lavigne, M. A. Salem, and C. Caloz, "Synthesis of electromagnetic metasurfaces: Principles and illustrations," *EPJ Appl. Metamater.*, vol. 2, p. 12, Oct. 2015.
[29] A. A. Elsakka, V. S. Asadchy, I. A. Faniayeu, S. N. Tcvetkova, and S. A. Tretyakov, "Multifunctional cascaded metamaterials: Integrated transmitarrays," *IEEE Trans. Antennas Propag.*, vol. 64, no. 10, pp. 4266–4276, Oct. 2016.
[30] D. Attwood, "Soft X-rays and extreme ultraviolet radiation," in *Soft X-Rays and Extreme Ultraviolet Radiation: Principles and Applications*. Cambridge, U.K.: Cambridge Univ. Press, 1999, pp. 337–363.
[31] A. Epstein and G. V. Eleftheriades, "Huygens' metasurfaces via the equivalence principle: Design and applications," *J. Opt. Soc. Amer. B*, vol. 33, no. 2, p. A31, Feb. 2016.
[32] N. M. Estakhri and A. Alù, "Wave-front transformation with gradient metasurfaces," *Phys. Rev. X*, vol. 6, no. 4, p. 41008, Oct. 2016.
[33] A. Jouadé, J. Bor, O. Lafond, and M. Himdi, "Millimeter-wave fresnel zone plate lens based on foam gradient index technological process," in *Proc. 10th Eur. Conf. Antennas Propag. (EuCAP)*, Apr. 2016, pp. 1–4.
[34] C. Pfeiffer and A. Grbic, "A printed, broadband Luneburg lens antenna," *IEEE Trans. Antennas Propag.*, vol. 58, no. 9, pp. 3055–3059, Sep. 2010.
[35] J. Kirz, "Phase zone plates for X rays and the extreme UV," *J. Opt. Soc. Amer.*, vol. 64, no. 3, pp. 301–309, 1974.
[36] I. Shishkin *et al.*, "Microwave platform as a valuable tool for characterization of nanophotonic devices," *Sci. Rep.*, vol. 6, no. 1, p. 35516, 2016.
[37] D. S. Filonov, A. S. Shalin, I. Iorsh, P. A. Belov, and P. Ginzburg, "Controlling electromagnetic scattering with wire metamaterial resonators," *J. Opt. Soc. Amer. A*, vol. 33, no. 10, pp. 1910–1916, Oct. 2016.
[38] D. Filonov, Y. Kramer, V. Kozlov, B. A. Malomed, and P. Ginzburg, "Resonant meta-atoms with nonlinearities on demand," *Appl. Phys. Lett.*, vol. 109, no. 11, p. 111904, Sep. 2016.